Elastic scattering and electron capture processes in collisions of $^{3}He^{2+}$ ion with CO molecule below 5 keV

Ashok Kumar Jha*, Shankar Kumar and Tinku Kumar

Department of Physics, Patna Science College, Patna University, Patna

*e-mail: ashok-physics@patnauniversity.ac.in

The single electron capture process in collisions of $^{3}He^{2+}$ ions with CO molecule have been studied theoretically using semiclassical collision methods in which the adiabatic potentials and nonadiabatic couplings were obtained using the multireference single- and double-excitation configuration-interaction (MRDCI) approach. The partial and total single electron capture cross sections have been obtained for energies between 0.6 to 6 keV. The calculated cross sections depend very sensitively on the molecular configuration, thus revealing a strong steric effect. The calculated single electron capture cross sections are in good agreement with the experimental measurements of Kusakabe *et al.* [Phys. Rev. A **73**, 022706 (2006)] and Čadež *et al*. [J. Phys. B: At. Mol. Opt. Phys. **35**, 2515 (2002)]. The present study provides a theoretical basis for the experimental measurements by interpreting the detailed collision dynamics.

I. INTRODUCTION

In last few decades there have been numerous important advances in the experimental and theoretical techniques which have significantly improved our understanding of various processes occurring in the astrophysical plasma [1]. The electron capture in collisions of slow multiply charged ion with atomic or molecular targets plays an important role in our understanding of mechanisms responsible for the emission of x-rays and extreme ultraviolet (EUV) photons from astrophysical plasmas [2, 3]. The emission lines of these multiply charged ions are used to provide direct information about the ionization structure of astrophysical objects. Protons and doubly ionized helium (He^{2+}) i.e. the α particle, are the primary ion

constituents of cosmic rays and the solar-wind. The helium ion was observed in outer space by an EUV scanner on the Mars Orbiter Planet-B [4]. The EUV satellite has performed detailed spectroscopic studies of comets in the vaccum ultraviolet (VUV) spectral range [5, 6]. The lines observed in the spectra have confirmed that electron capture processes are present in the comets. Some spectral lines of helium appeared to be very bright, and well separated from other lines. They are the result of de-excitation subsequent to electron capture into excited states of singly charged or neutral helium. The luminosities of these lines have been determined from these observations. To interpret them, one needs to know the underlying electron capture and subsequent line emission cross sections.

Recently measured He^+ emission lines from the comet Hyakutake [5] has led us to calculate total and partial cross sections for the collision of He^{2+} ion with the CO molecule, since the latter is one of the major constituents of the comet's neutral atmosphere near the sun. The processes we are concerned with are as follows [7]:

$$\begin{aligned} He^{2+} + CO &\rightarrow He^+(1s^2S) + CO^+(\Sigma) + \Delta E \quad \text{(dissociative)}, \\ &\rightarrow He^+(n \geq 2) + CO^+(\Sigma) \pm \Delta E_1 \ \text{(non-dissociative)}. \end{aligned}$$

where n is the principal quantum number, ΔE and ΔE_1 are the energy defects for individual product channels and CO^+ (Σ) includes final bound or dissociative molecular states. The collision of He^{2+} ion with the CO molecule has been widely studied experimentally [7-12] but limited systematic theoretical work has been reported [8]. The agreement between the experimental measurements and theoretical calculations is not satisfactory and hence, so far no clear explanation for the observed results has been given [8].

Therefore, in the present study, the impact-parameter method [13] has been used to study the single electron capture (SEC) process. The adopted adiabatic potentials and nonadiabatic couplings were obtained with the multireference single- and double-excitation configuration interaction (MRDCI) approach [14-21]. In order to provide suitably accurate results, we have used an optimization method for the atomic basis sets used in the MRDCI calculation for multiply charged ions. The calculation of the ion-molecule collisions is based on the perturbed stationary state (PSS) model [22] in which the basis functions are constructed from the molecular orbitals.

The partial and total SEC cross sections have been calculated for collision energies lying between 0.6 to 6 keV, corresponding to a solar-wind ion velocity of about 3 keV at low

heliographic latitudes [23]. The calculated electron capture cross sections have been compared with the available experimental data [7, 8] and it has been shown that the impact parameter method provides cross sections which are in good agreement with experimental measurements [7, 8] in the range of energy considered in the present work.

II. THEORETICAL MODELS

A. Molecular state

The geometry for the collision of He^{2+} ion with CO molecule is shown in Fig. 1. The He^{2+} + CO system has been described by the internal Jacobi coordinates {R, r, α} with the origin at the center of mass of the CO molecule. The *ab initio* calculations have been performed using the MRDCI method [14-21] for three different directions of approach of He^{2+} ion towards the CO molecule. In the linear conformation, the He^{2+} ion approaches the carbon and oxygen ends of CO molecule at an angle α = 0 and 180°, respectively. In these cases, the calculations are done in the C_{2v} subgroup (the highest Abelian subgroup) of the $C_{\infty v}$ point group. In the perpendicular approach (α = 90°), He^{2+} ion approaches the center of mass of CO vertically along the Z axis. The only symmetry plane for the system is the YZ plane (C_s point group) and the electronic states are classified according to the two irreducible representations A' and A'' of the C_s point group. In this case the interactions are through radial couplings between A' states, the X component of the rotational couplings between the A' states, and the Y and Z components of the rotational couplings between the A' and A'' states. Other interactions have been excluded due to symmetry constraints.

In all three directions of approach, the origin of the scattering coordinates is located at the center of mass of the $[HeCO]^{2+}$ system. In the collision energy range considered in the present work, the collision time is much shorter than the relaxation time of the target CO. Hence, the molecular state calculation has been performed with CO internuclear distance fixed at 2.13222 a_0 corresponding to the equilibrium geometry of the ground state of CO molecule.

The basis set employed in this work consists of contracted Cartesian Gaussian functions. For carbon the aug-cc-pVQZ [24] basis set [6*s*, 5*p*, 4*d*, 3*f*, 2*g*] is contracted to [6*s*, 5*p*, 4*d*, 3*f*] augmented with two diffuse *s* (α_s = 0.0230000 and 0.0055000 a_0^{-2}), two diffuse *p* (α_p = 0.021000 and 0.0049000 a_0^{-2})and two diffuse *d* (α_d = 0.0150000 and 0.0032000 a_0^{-2}). For

oxygen the aug-cc-pVQZ [24] basis set [6*s*, 5*p*, 4*d*, 3*f*, 2*g*] is contracted to [6*s*, 5*p*, 4*d*, 3*f*] augmented with two diffuse *s* (α_s = 0.0320000 and 0.0022000 a_0^{-2}) two diffuse *p* (α_p = 0.0310000 and 0.0011000 a_0^{-2}) and two diffuse *d* (α_d = 0.0150000 and 0.0032000 a_0^{-2}) are added into this contracted basis set. For helium optimized aug-cc-pVQZ [25] basis set [10*s*, 5*p*, 2*d*, 1*f*] is used.

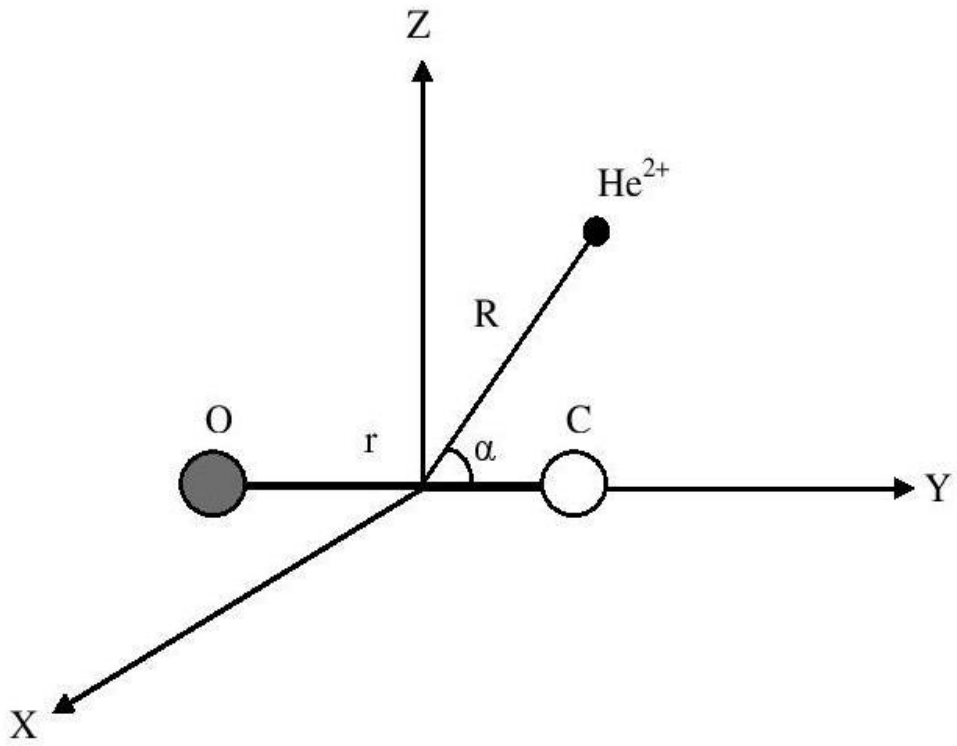

FIG. 1. Internal coordinates for the $[HeCO]^{2+}$ system.

A self-consistent field (SCF) calculation has been carried out for the lowest-energy $^1A_1$ state at each internuclear distance considered for all the three directions of approach. The resulting molecular orbitals (MOs) form the orthonormal one-electron basis for the subsequent CI treatments.

The adiabatic MRDCI energies have been calculated at 173 internuclear separations in the range $1.5 \leq R \leq 50.0$ a_0 (R being the distance of He^{2+} from the center of CO. The MRDCI method is employed with configuration selection and perturbative energy corrections [14-21].

Table I: Number of reference configurations N_{ref} and number of roots N_{root} treated in each irreducible representation and the corresponding number of generated (N_{tot}) and selected (N_{sel}) symmetry-adapted functions with analog of Davidson-Langhoff correction for a threshold of 1.0×10^{-6} hartree. Note that R is the distance between He^{2+} ion and CO center of mass.

State	N_{ref}	N_{tot}	N_{sel}	N_{root}	$\Sigma_p\, c_p^2$
carbon end	R = 2.1 a_0				
$^1A_1$	117	25107571	152860	8	0.91925
$^1B_1$	131	36530868	130437	5	0.91400
$^1A_2$	58	19913451	100128	4	0.91925
$^3A_1$	122	56874767	132811	6	0.91783
$^3B_1$	131	66373749	123435	5	0.91880
$^3A_2$	58	36315855	100829	4	0.91825
oxygen end	R = 2.7 a_0				
$^1A_1$	108	24130542	159236	8	0.92560
$^1B_1$	72	19081874	141719	5	0.92100
$^1A_2$	41	12479242	114371	4	0.91875
$^3A_1$	113	54168588	128649	6	0.92980
$^3B_1$	124	65232445	150152	5	0.92960
$^3A_2$	70	46421304	119775	4	0.92790
center of mass	R = 3.5 a_0				
$^1A'$	214	76191198	193952	10	0.92620
$^1A''$	127	60828104	160514	6	0.92050
$^3A'$	217	149263062	201955	10	0.92740
$^3A''$	154	134429332	149371	6	0.92616

A set of reference configurations is chosen based on a preliminary scan of the wave functions of the lowest roots of a given symmetry at representative internuclear distances.

A selection threshold of T = 1.0×10^{-6} hartree is employed to divide the generated configurations into two sets based on their ability to lower the total energy of a given root relative to that obtained in the small reference secular equations. The details regarding the numbers of reference configurations, roots selected and the corresponding sizes of the generated and selected CI spaces are given in Table I. The calculations are carried out in the C_{2v} subgroup of the $C_{\infty v}$ point group, but the MOs themselves transform according to the irreducible representations of $D_{\infty h}$ linear symmetry, making identification of the resulting CI eigenfunctions straightforward.

The configuration interaction (CI) treatment has been carried out by employing the Table CI method [19-21] for efficient treatment of the various open-shell cases which arise because of the single and double substitutions relative to the reference configurations. Sums of squared coefficients of reference configurations $\Sigma_p \, c_p^2$ for each of the lowest roots are also given in Table I. This quantity is an indication of the quality of the choice of the reference species in each case. Typically values of 0.929–0.914 are found, which is a satisfactory range for CI treatments with only ten active electrons (the carbon 1*s* shell and oxygen 1*s* shell are always doubly occupied). The $\Sigma_p \, c_p^2$ values are also employed in the multireference analog to the Davidson correction [26, 27] to the energy of each root in order to estimate the effect of higher excitations and therefore to obtain the corresponding full CI energy to a good approximation.

The calculated first ionization potential of CO molecule, giving rise to CO^+ ($^2\Sigma^+$), is 13.6692 eV, which agrees well with the experimental value of 13.99 eV determined from photoelectron spectroscopy [28]. The calculated energy differences between the single electron capture channel, He^+ (1*s* ^2S) + CO^+ (X $^2\Sigma^+$) and the entry channel, He^{2+} + CO (X $^1\Sigma^+$) at R = 50 a_0 are 2.20786 and 2.24599 eV for He^{2+} ion approaching the carbon and oxygen ends, respectively. For the triplet manifold the calculated energy differences for the single electron capture channel, He^+ (1*s* ^2S) + CO^+ (X $^2\Sigma^+$) and the entry channel, He^{2+} + CO (X $^3\Sigma^+$) are 9.2834 and 9.2913 eV for He^{2+} ion approaching the carbon and oxygen ends, respectively. For the perpendicular approach, the asymptotic energy difference could not be calculated as the entry channel lies much above the calculated adiabatic potentials.

Having used the optimized basis, the radial coupling matrix elements between all pairs of states of same symmetry have been calculated by applying a finite-difference method [29]

$$A_{ij} = < \psi_i | \frac{\partial}{\partial R} | \psi_j > = \lim_{\Delta R \to 0} \frac{1}{\Delta R} < \psi_i(R) | \psi_i(R + \Delta R) >,$$

with a step size of 0.0002 a_0 and the electronic coordinate origin at the center of mass of the $[HeCO]^{2+}$ system. The rotational couplings between states of angular momentum $\Delta\Lambda = \pm 1$ have been calculated from the angular momentum tensor using a standard procedure [30].

B. Scattering calculation

The scattering calculation has been performed in the keV region, where it has been found that the straight-line trajectories are satisfactory [31] and semiclassical approaches have been applied with good accuracy [32]. The computations have been performed using the EIKONX program [13] based on an efficient propagator method [33].

For He^{2+} ions of keV energy, the collision times are approximately of the order of 10^{-16} s, whereas the molecular rotation and vibration times are typically of the order of 10^{-11} and 10^{-14} s, respectively [34]. Hence, the internuclear distance between the C and O atoms can be assumed to remain fixed during the collision, i.e. the Franck–Condon (FC) principle can be applied as the molecular rotation and vibration time are longer than the collision time. Cross sections corresponding to purely electronic transitions are thus determined by solving the impact parameter equation as in the usual ion-atom approach, considering the internuclear distance of the molecular target fixed in a given geometry.

The electronic transitions between the molecular states are mainly governed by the nonadiabatic radial and rotational coupling matrix elements. Hence, the coupled equations have been solved taking account of all the relevant radial and rotational couplings. In the present study, electron translation factors (ETFs), which are often used to ensure that the cross sections are independent of the origin of coordinates, have been used. The ETFs have been evaluated in the approximation of common translation factors (CTFs) [35]. The influence of ETFs is expected to be very low in the energy range considered in the present work, but their inclusion ensures that the correct scattering boundary conditions are satisfied.

The influence of spin-orbit couplings is expected to be low in the range of energy considered in the present work. Hence, singlet and triplet states have been considered

separately. Singlet states included in the dynamical calculations are: the entry channel 2 $^1\Sigma^+$ [He^{2+} + CO ($X\ ^1\Sigma^+$)] and SEC channels: 1 $^1\Sigma^+$ [He^+ ($1s\ ^2S$) + CO^+ ($X\ ^2\Sigma^+$)], 3 $^1\Sigma^+$ [He^+ (n=2) + CO^+ ($X\ ^2\Sigma^+$)], 4 $^1\Sigma^+$ [He^+ (n=3) + CO^+ ($X\ ^2\Sigma^+$)], 5 $^1\Sigma^+$ [He^+ (n=3) + CO^+ ($A\ ^2\Sigma^+$)], 1 $^1\Pi$ [He^+ (n=2) + CO^+ ($A\ ^2\Pi$), 2 $^1\Pi$ [He^+ (n=3) + CO^+ ($A\ ^2\Pi$)]. Triplet states included in the dynamical calculations are: the entry channel 5 $^3\Sigma^+$ [He^{2+} + CO ($X\ ^3\Sigma^+$)] and SEC channels: 1 $^3\Sigma^+$ [He^+ ($1s\ ^2S$) + CO^+ ($X\ ^2\Sigma^+$)], 2 $^3\Sigma^+$ [He^+ ($1s\ ^2S$) + CO^+ ($A\ ^2\Sigma^+$)], 3 $^3\Sigma^+$ [He^+ (n=2) + CO^+ ($X\ ^2\Sigma^+$)], 4 $^3\Sigma^+$ [He^+ (n=2) + CO^+ ($A\ ^2\Sigma^+$)], 1 $^3\Pi$ [He^+ ($1s\ ^2S$) + CO^+ ($A\ ^2\Pi$)], 2 $^3\Pi$ [He^+ (n=2) + CO^+ ($A\ ^2\Pi$)].

III. RESULTS

A. Adiabatic potentials and nonadiabatic couplings

Rotational couplings are considered relative to the entry channel symmetries ($^1\Sigma^+$ and $^3\Sigma^+$), and thus $^1\Pi$ and $^3\Pi$ states have also been included in the collision dynamics. The adiabatic potential energy curves for He^{2+} ion approaching the oxygen (α = 180°) end of the CO molecule (singlet states) are shown in Fig. 2. The 2 $^1\Sigma^+$ state corresponds to the entry He^{2+}/CO channel whereas all the remaining states correspond to He^+/CO^+ single electron capture channels.

The 1 $^1\Sigma^+$ and 2 $^1\Sigma^+$ states show an avoided crossing lying between R = 8 to 9 a_0 for He^{2+} ion approaching the oxygen end of the CO molecule, whereas for the carbon (α = 0°) end the avoided crossings are observed beyond R = 9.5 a_0. The 2 $^1\Sigma^+$ and 3 $^1\Sigma^+$ states show an avoided crossing near R = 2.2 a_0 for the carbon end, whereas there is very weak (or no) avoided crossing between these states for the oxygen end of the CO molecule. For both termini the 4 $^1\Sigma^+$ and 5 $^1\Sigma^+$ states exhibit multiple avoided crossings and they are expected to play a significant role in the SEC process in the high-energy collisions. The curve crossings between the entry channel 2 $^1\Sigma^+$ and SEC channel 1 $^1\Pi$ suggest that there is a significant contribution from the 1 $^1\Pi$ state in the SEC process, whereas the curve crossing between the 2 $^1\Pi$ state and high-lying 4 $^1\Sigma^+$ and 5 $^1\Sigma^+$ states contributes to the flux redistribution in high-energy collisions.

For the triplet states the adiabatic potentials for He^{2+} ion approaching the oxygen end of the CO molecule are shown in Fig. 3. The entry channel (He^{2+}/CO) is 5 $^3\Sigma^+$, whereas all other states correspond to SEC (He^+/CO^+) channels. As in the case of singlet states, the adiabatic potentials for triplet states for both termini (carbon and oxygen) exhibit some distinctive

characteristics. For the oxygen end, the 5 $^3\Sigma^+$ and 4 $^3\Sigma^+$ states show a strong avoided crossing near R = 2.8 a_0 and other smoothly avoided crossings between R = 3.5 - 4 a_0, 4.5 - 5.5 a_0 and beyond 9 a_0. By contrast, for the carbon end (α = 0°) these states show a smooth avoided crossing below R = 2 a_0, a very weak avoided crossing near R = 5.5 a_0 and a weak avoided crossing around R = 10 a_0. The 3 $^3\Sigma^+$ and 4 $^3\Sigma^+$ states for the carbon-end approach show strong avoided crossings near R = 2.2, 4.1 and 7.5 a_0, whereas for the oxygen end these states (5 $^3\Sigma^+$ and 4 $^3\Sigma^+$) undergo a smooth avoided crossing below R= 2.5 a_0, and a strong avoided crossing near R = 4.2, 6.0 and 6.5 a_0. For both ends, the 3 $^3\Sigma^+$, 2 $^3\Sigma^+$ and 1 $^3\Sigma^+$ states exhibit very weak or no avoided crossings.

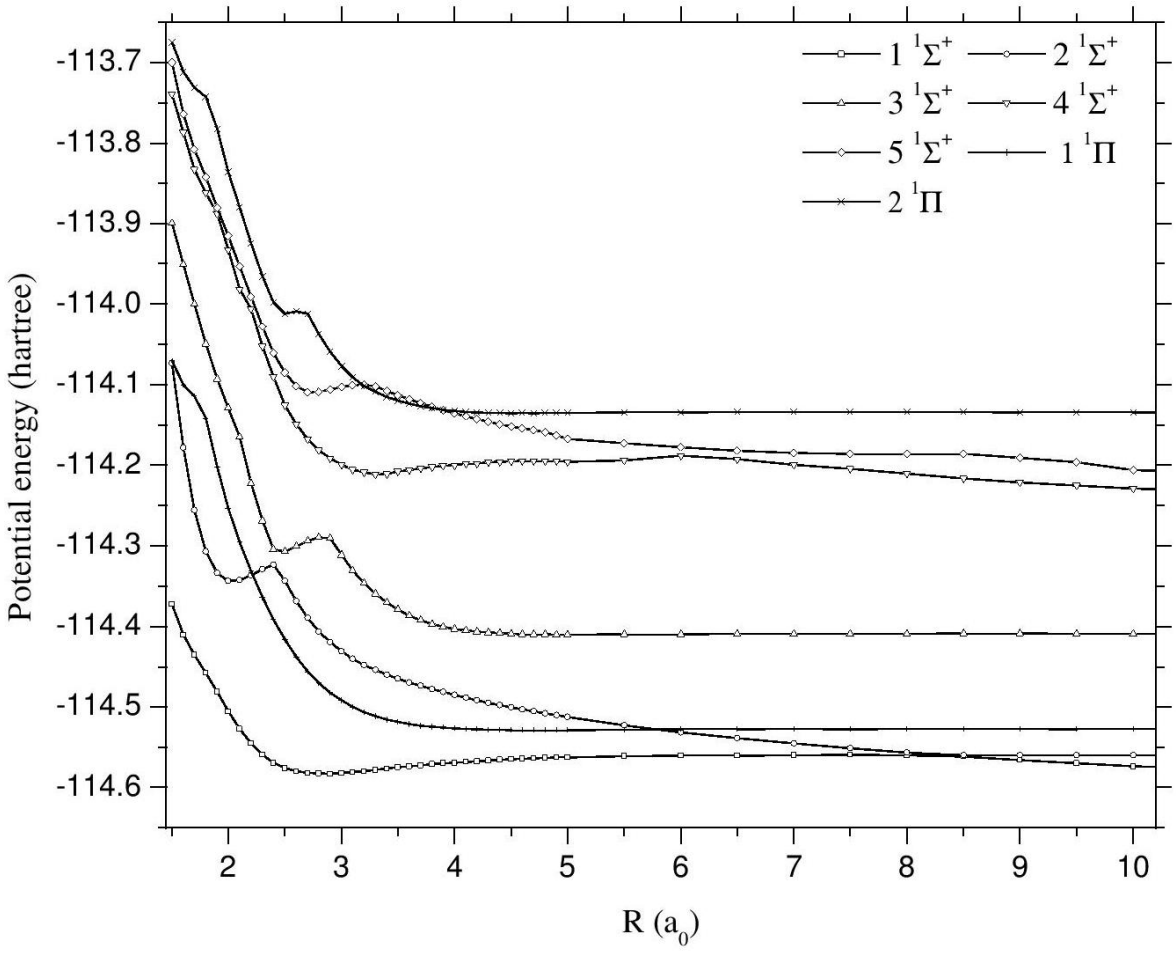

FIG. 2. Adiabatic potential energy curves for the $^1\Sigma^+$ and $^1\Pi$ (singlet) states of the $[HeCO]^{2+}$ system at equilibrium, α = 180°.

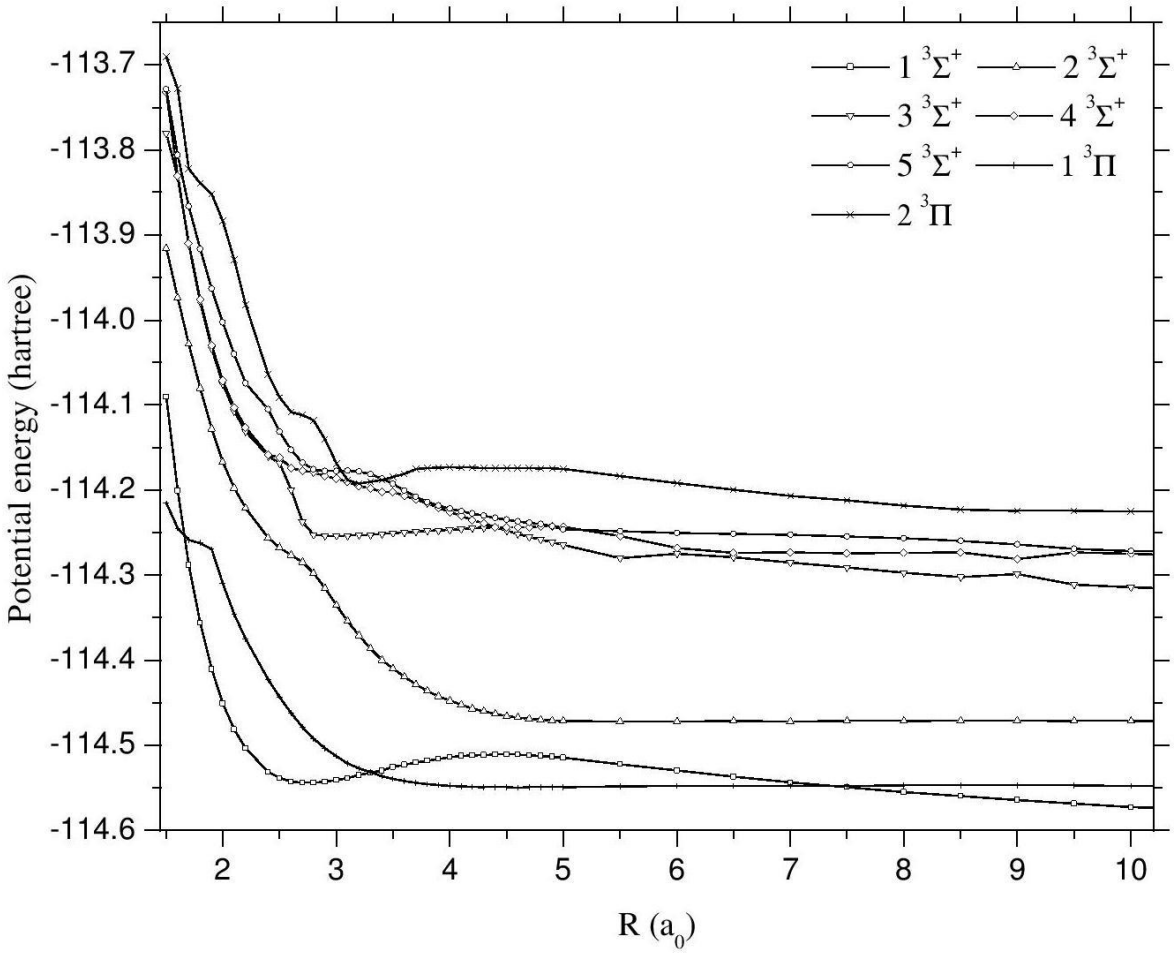

FIG. 3. Adiabatic potential energy curves for the $^3\Sigma^+$ and $^3\Pi$ (triplet) states of the $[HeCO]^{2+}$ system at equilibrium, $\alpha = 180°$.

The curve crossings between the 2 $^3\Pi$ and 5 $^3\Sigma^+$ states suggest an important role played by the 2 $^3\Pi$ state in the SEC process, whereas the curve crossings between the 1 $^3\Pi$ and 1 $^3\Sigma^+$ states play a significant role in flux redistribution. For both singlet and triplet states the amount of mixing is comparatively weaker for He^{2+} ion approaching the carbon end than for the oxygen end of the CO molecule. Hence, a strong steric effect is expected to play an important role in the SEC process.

In the adiabatic potential energy curves for the He^{2+} ion approaching the center of mass ($\alpha = 90°$) of the CO molecule, the ground state entry channel (He^{2+}/CO) lies much above the calculated potentials and hence it has not been included in the scattering calculation.

Since there are many channels considered in the present calculation and as the radial couplings between non-adjacent states are much smaller than those between the adjacent states, only the radial couplings for the adjacent channels of the $^1\Sigma^+$ (singlet) and $^3\Sigma^+$ (triplet) states are shown as an illustration. The radial couplings for the adjacent $^1\Sigma^+$ (singlet) and $^3\Sigma^+$ (triplet) states for He^{2+} ion approaching the oxygen ($\alpha = 180°$) end of the CO molecule are shown in Figs. 4 and 5, respectively. There is significant change in positions, nature and magnitudes of the radial couplings with the change in the orientation of the He^{2+} projectile towards the CO molecule.

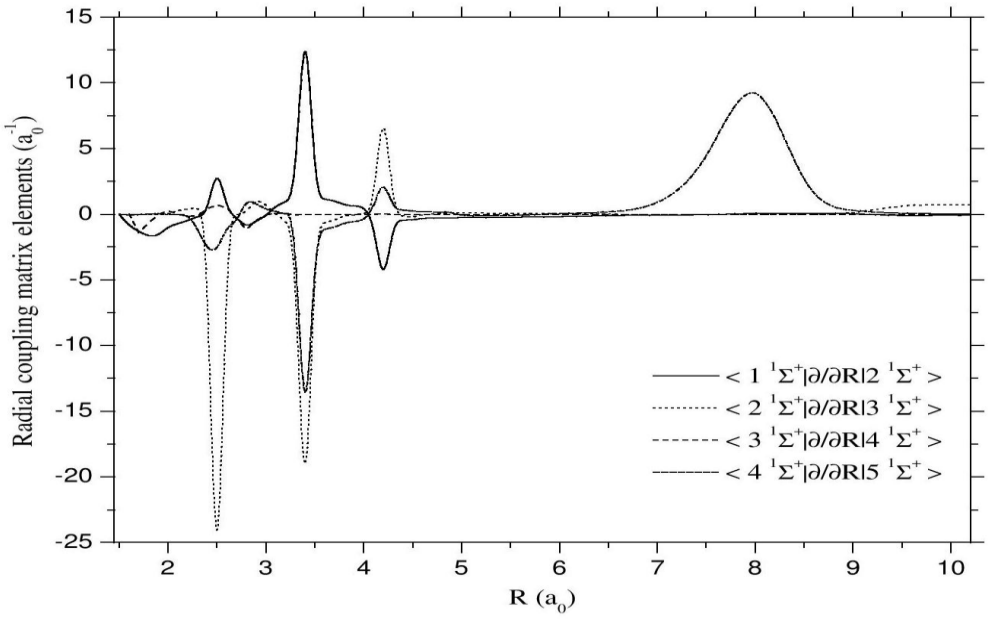

FIG. 4. Nonadiabatic radial couplings for the adjacent $^1\Sigma^+$ (singlet) states of the $[HeCO]^{2+}$ system at equilibrium, $\alpha = 180°$.

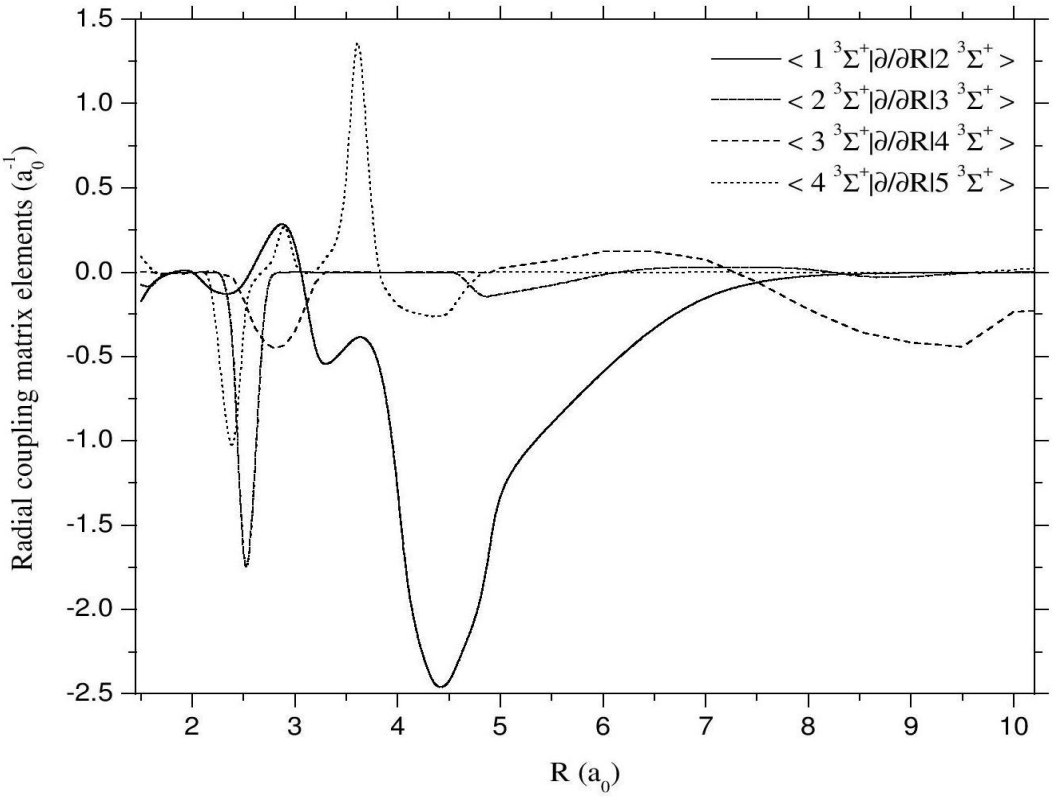

FIG. 5. Nonadiabatic radial couplings for the adjacent $^3\Sigma^+$ (triplet) states of the $[HeCO]^{2+}$ system at equilibrium, $\alpha = 180°$.

The rotational couplings between the adjacent $^{1,3}\Sigma^+$ and $^{1,3}\Pi$ states for the oxygen (α = 180°) end of CO molecule are shown in Figs. 6 and 7, respectively, for the singlet and triplet states. The rotational couplings between two states corresponding to molecular fragments having the same number of electrons such as, $< 3\ ^1\Sigma^+|\ iL_y\ |\ 1\ ^1\Pi>$ and $< 2\ ^3\Sigma^+|\ iL_y\ |\ 1\ ^3\Pi>$ have a finite constant value at large R. For the states corresponding to molecular fragments with different configurations, such as $< 1\ ^1\Sigma^+|\ iL_y\ |\ 1\ ^1\Pi>$ and $< 1\ ^3\Sigma^+|\ iL_y\ |\ 1\ ^3\Pi>$, the rotational couplings approach zero at large R. Due to nonadiabatic interactions between the adjacent states, the rotational couplings are not smooth near the avoided crossings.

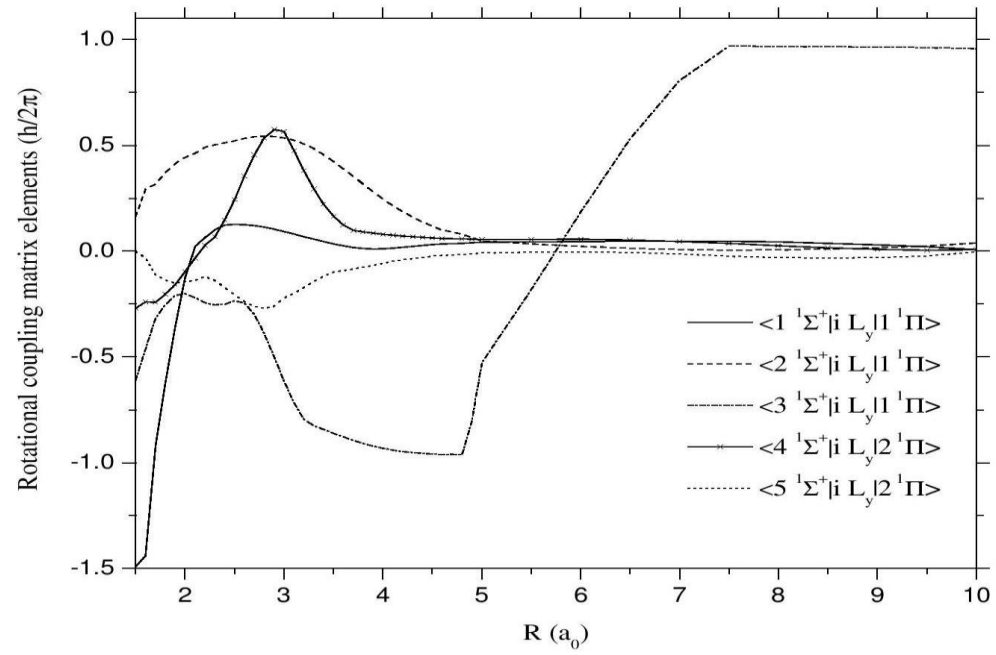

FIG. 6. Nonadiabatic rotational couplings for the adjacent $^1\Sigma^+$ and $^1\Pi$ (singlet) states of the $[HeCO]^{2+}$ system at equilibrium, $\alpha = 180°$.

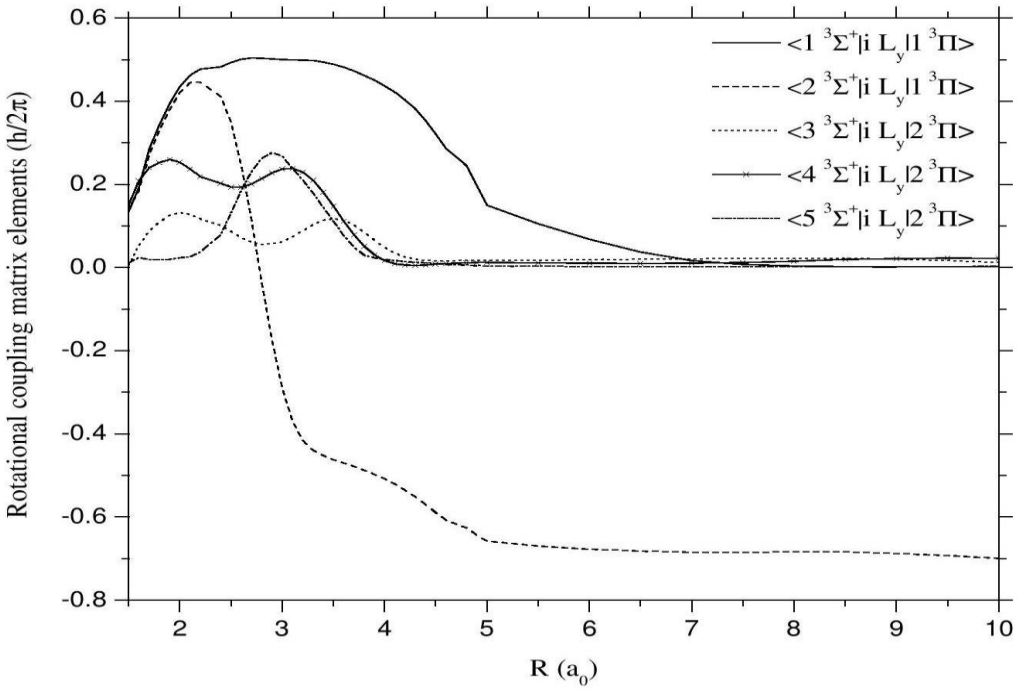

FIG. 7. Nonadiabatic rotational couplings for the adjacent $^3\Sigma^+$ and $^3\Pi$ (triplet) states of the $[HeCO]^{2+}$ system at equilibrium, $\alpha = 180°$.

B. Cross sections

The collision dynamics for the $[HeCO]^{2+}$ system has been performed in the energy range of 0.6 to 6.0 keV. The spin-orbit effects have been neglected in the energy range of interest so triplet and singlet manifolds have been considered separately. According to the statistical weight, the triplet manifold accounts for 3/4 of the population of the ground state entry channel, against 1/4 for the singlet manifold. To understand the effect of molecular orientation on cross sections, the calculation has been performed for He^{2+} ion approaching both the carbon and oxygen termini of the CO molecule.

1. Partial cross sections for each individual level

Partial SEC cross sections for He^{2+} ion approaching the oxygen end ($\alpha = 180°$) of the CO molecule (singlet states) are shown in Fig. 8. For both the orientations of the He^{2+} projectile towards the CO molecule, the 1 $^1\Sigma^+$ [He^+ (1*s* ^2S) + CO^+ (*X* $^2\Sigma^+$)] state has a dominant contribution in the SEC process below 3 keV, illustrating the important role played by radial coupling matrix elements between the 1 $^1\Sigma^+$ state and the entry channel 2 $^1\Sigma^+$ [He^{2+} + CO (*X* $^1\Sigma^+$)] in low energy collisions. The 3 $^1\Sigma^+$ [He^+ (*n*=2) + CO^+ (*X* $^2\Sigma^+$)] state has an important contribution in the SEC process and it increases with collision energy. This reflects the fact that the contribution of the radial coupling matrix elements between the 3 $^1\Sigma^+$ and the entry channel 2 $^1\Sigma^+$ also increases with collision energy. For the carbon end ($\alpha = 0°$), the 1 $^1\Pi$ [He^+ (*n*=2) + CO^+ (*A* $^2\Pi$)] state also has a significant contribution in the SEC process and it again increases with collision energy. The same holds for the rotational coupling matrix element between the 1 $^1\Pi$ [He^+ (*n*=2) + CO^+ (*A* $^2\Pi$)] state and the 2 $^1\Sigma^+$ entry channel. By contrast, the 1 $^1\Pi$ state has comparatively low contribution in the SEC for the oxygen end ($\alpha = 0°$) whereas a significant contribution is observed in high-energy collisions. For both the orientations, the SEC channels 4 $^1\Sigma^+$ [He^+ (*n*=3) + CO^+ (*X* $^2\Sigma^+$)], 5 $^1\Sigma^+$ [He^+ (*n*=3) + CO^+ (*A* $^2\Sigma^+$)] and 5 $^1\Pi$ [He^+ (*n*=3) + CO^+ (*A* $^2\Pi$)] play only a secondary role in the SEC process in low- to intermediate-energy collisions. For the oxygen end, the 5 $^1\Pi$ state has a significant contribution in the SEC process in intermediate- to high-energy collisions.

Partial SEC cross sections for He^{2+} ion approaching the oxygen end (triplet states) are shown in Fig. 9. The 1 $^3\Pi$ [He^+ (1*s* ^2S) + CO^+ (*A* $^2\Pi$)] state has a dominant contribution in the

SEC process and it increases with collision energy. Hence, rotational coupling matrix elements between the 1 $^3\Pi$ state and the entry channel 6 $^3\Sigma^+$ [He^{2+} + CO (X $^3\Sigma^+$)] are seen to play an important role. The 4 $^3\Sigma^+$ [He^+ (n=2) + CO^+ (X $^2\Sigma^+$)] state has an important contribution in the SEC process and shows a low dependence on collision energy below 4 keV. Thus, radial coupling matrix elements between the 4 $^3\Sigma^+$ state and the entry channel 6 $^3\Sigma^+$ have a significant contribution in the SEC process in high-energy collisions. The SEC channels, 1 $^3\Sigma^+$ [He^+ (1s ^2S) + CO^+ (X $^3\Sigma^+$)] and 2 $^3\Sigma^+$ [He^+ (1s ^2S) + CO^+ (A $^2\Sigma^+$)], have a significant contribution in the electron capture process but their contribution decreases with collision energy. The 5 $^3\Sigma^+$ [He^+ (n=2) + CO^+ (A $^2\Sigma^+$)] state has only a small contribution in low-energy collisions but it increases with collision energy. The 5 $^3\Pi$ [He^+ (n=2) + CO^+ (A $^2\Pi$)] state plays a secondary role in the SEC process in low- to intermediate-energy collisions.

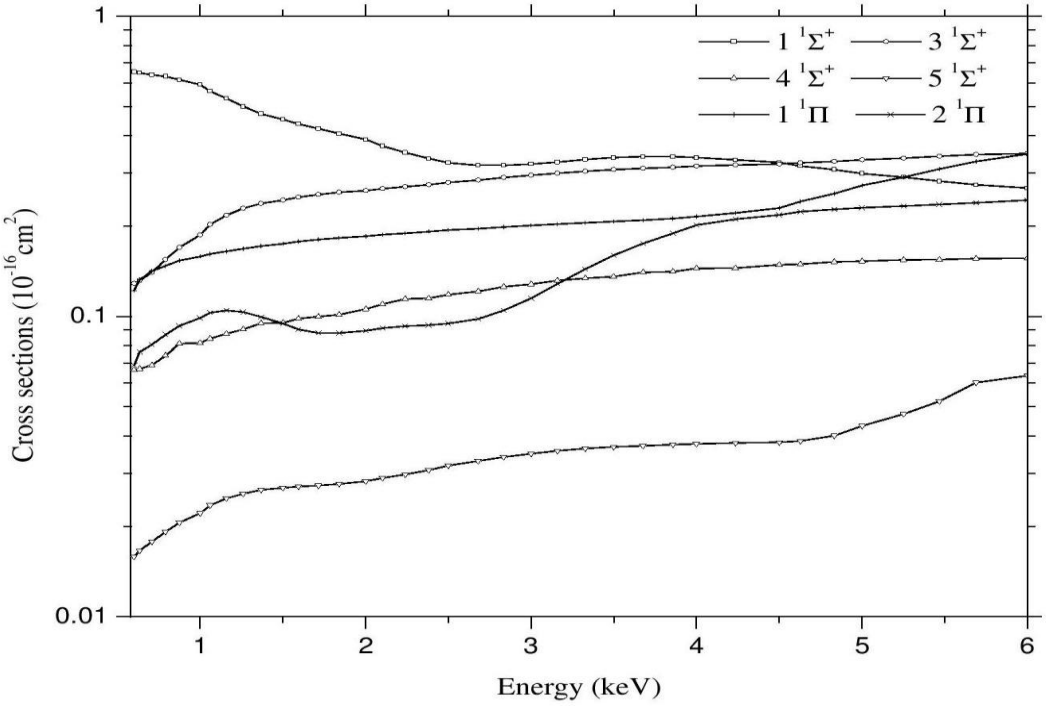

FIG. 8 Partial SEC cross sections for the $^1\Sigma^+$ and $^1\Pi$ (singlet) states of the $[HeCO]^{2+}$ system at equilibrium, $\alpha = 180°$.

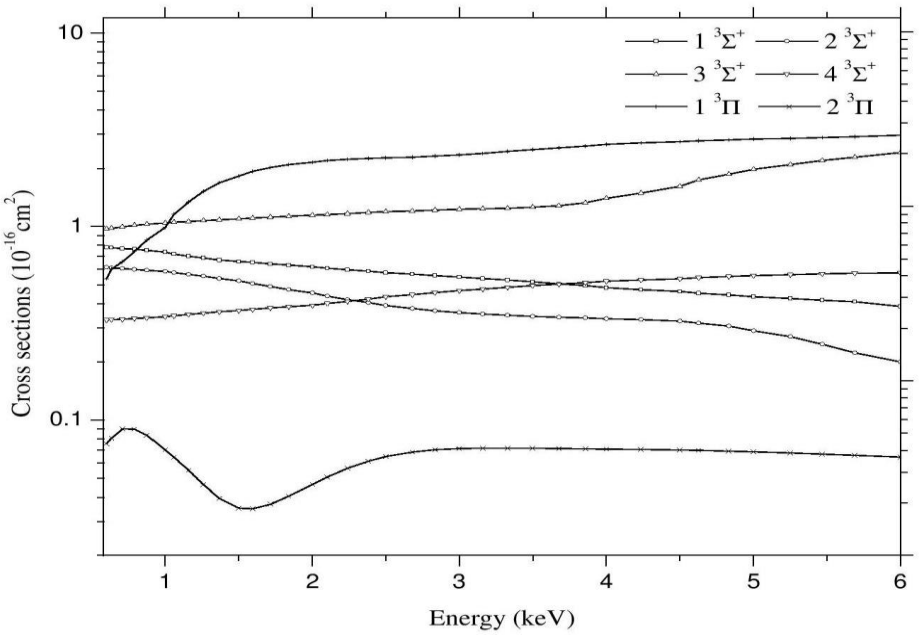

FIG. 9. Partial SEC cross sections for the $^3\Sigma^+$ and $^3\Pi$ (triplet) states of the $[HeCO]^{2+}$ system at equilibrium, $\alpha = 180°$.

In the partial SEC cross sections for He^{2+} ion approaching the carbon end (triplet states), the 1 $^3\Pi$ [He^+ (1*s* ^2S) + CO^+ (*A* $^2\Pi$)] state makes a dominant contribution in the SEC process which increases with collision energy, emphasizing the important role played by the rotational coupling matrix elements between the 1 $^3\Pi$ state and the entry channel 5 $^3\Sigma^+$ [He^{2+} + CO (*X* $^3\Sigma^+$)] in the SEC process. The 4 $^3\Sigma^+$ [He^+ (*n*=2) + CO^+ (*X* $^2\Sigma^+$)] state has a small effect on the SEC process, showing a weak dependence on collision energy below 3.5 keV. Above this energy, the contribution of 4 $^3\Sigma^+$ increases with collision energy. Hence, the radial coupling matrix element between the 4 $^3\Sigma^+$ state and the entry channel 5 $^3\Sigma^+$ makes a significant contribution to the SEC process in high-energy collisions. The 2 $^3\Sigma^+$ [He^+ (1*s* ^2S) + CO^+ (*A* $^2\Sigma^+$)] state has a small influence on the SEC process and its contribution increases with collision energy below 2 keV. Above this energy, the 2 $^3\Sigma^+$ state in the SEC process shows very low dependence on collision energy. The 1 $^3\Sigma^+$ [He^+ (1*s* ^2S) + CO^+ (*X* $^3\Sigma^+$)], 5 $^3\Sigma^+$ [He^+ (*n*=2) + CO^+ (*A* $^2\Sigma^+$)] and 5 $^3\Pi$ [He^+ (*n*=2) + CO^+ (*A* $^2\Pi$)] states have only a very low contribution to the SEC process in low- to intermediate-energy collisions.

The oscillations observed in partial cross sections of these states arise due to interferences between these states. The computed partial cross sections show an important contribution of

the He^+ ($1s\ ^2S$) state in the SEC process in the low- to intermediate-energy collisions and a significant contribution of He^+ (n=2) state in intermediate- to high-energy collisions. These observations are in good agreement with the experimental measurements of Kearns *et al.* [7]. Although partial cross sections for the perpendicular approach ($\alpha = 90°$) of He^{2+} towards the CO molecule could not be calculated, the partial cross sections obtained for the two modes of approach (carbon and oxygen termini) illustrate that there is a strong steric effect in the collision dynamics.

2. Total cross sections

Total SEC cross sections for He^{2+} ion approaching the carbon and the oxygen ends of CO molecule have been shown in Fig. 10. Total electron capture cross sections for the oxygen end increases with collision energy, whereas for the carbon end total electron capture cross sections increases slowly with collision energy. It is evident from the curves that the SEC process is favoured more towards the oxygen end. Thus, the calculated SEC cross sections are highly dependent on molecular orientation.

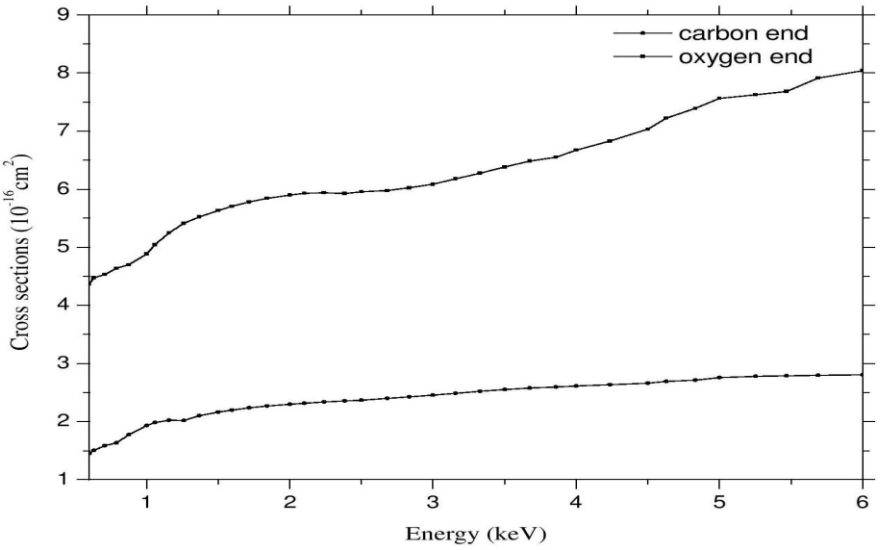

FIG. 10. Total SEC cross sections for different orientations of the He^{2+} projectile towards CO molecule at equilibrium.

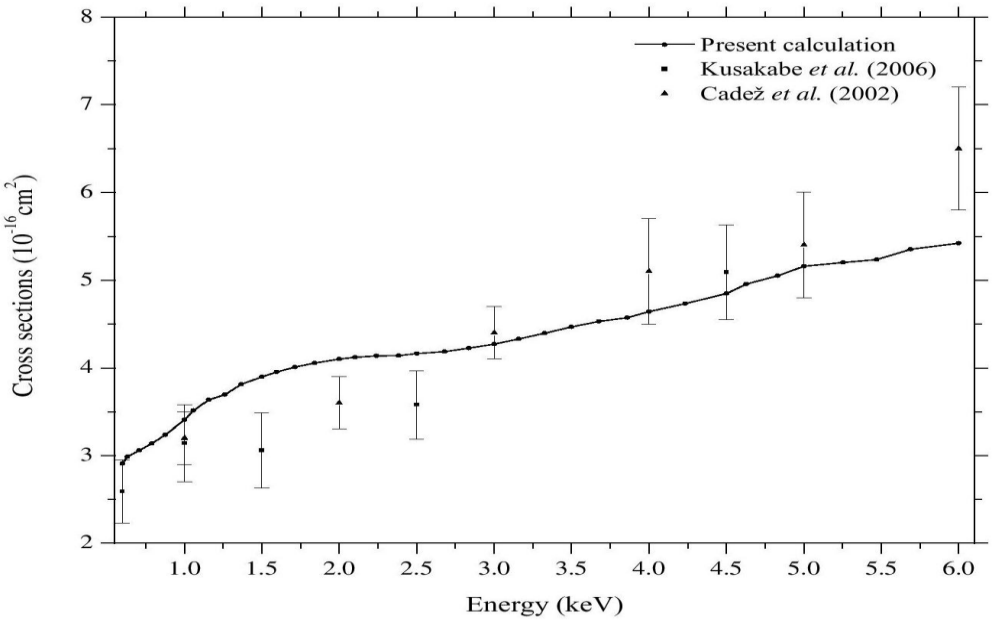

FIG. 11. Total SEC cross sections averaged over two different orientations of the He^{2+} projectile towards CO molecule at equilibrium; filled circles with solid line, the present calculation; filled rectangles with error bars, the measurements of Kusakabe *et al.* [8]; filled triangles with error bars, the measurements of Čadež *et al*. [9].

Finally, the computed total SEC cross sections averaged over two molecular orientations (carbon and oxygen termini) obtained in the present work and experimental measurements of Kusakabe *et al.* [8] and Čadež *et al*. [9] have been compared in the Fig. 11. In general, the overall agreement between the present calculations and the two experimental results is found to be very good. In the range of energy considered in the present study, our calculated SEC cross sections increase with collision energy. The energy dependence of the calculated cross sections agrees both qualitatively and quantitatively with the experimental measurements. Previously reported theoretical results of Kusakabe *et al.* [8] were smaller by 50 % than their experimental measurements. Thus, the SEC cross sections obtained in the present study are a significant improvement over the previous theoretical calculations. The agreement between the theoretical and experimental results is expected to improve with the inclusion of SEC cross sections for the perpendicular approach of the He^{2+} ion towards the CO molecule.

C. Fragmentation

Although in the present study no rigorous analysis of fragmentation of the CO molecule caused by He^{2+} ion impact was done, we briefly outline the possible mechanisms and consequences of fragmentation processes. For the collision of He^{2+} ion with CO molecule the energy difference between the entry channel He^{2+} + CO ($X\ ^1\Sigma^+$) and the SEC channel He^+ ($1s\ ^2S$) + CO^+ [dissociative states] lies in the range of 0 to 20 eV [7]. The energy difference between the entry channel (He^{2+}/CO) and the SEC channel, He^+ (n=2) + CO^+ ($X\ ^2\Sigma^+$) is small (-0.42 eV) [7]. Radial coupling matrix elements between the entry channel and single electron capture [He^+ ($1s\ ^2S$) + CO^+] channels are sizable. Thus, the electron capture into the [He^+ ($1s\ ^2S$) + CO^+] channel is very effective in low energy collisions. The final products of the electron capture process depend on the energy transfer to CO^+ in the collision process. The lowest CO^+ state has a binding energy of about 8.3 eV [36] and has a nearly identical equilibrium internuclear distance as that of the CO ground state. Therefore, in view of the FC principle, it is likely that most of the CO^+ ions produced in the SEC into the He^+ (n=2) will be into the low-lying bound states of CO^+ which are quite stable. The SEC into the He^+ ($1s\ ^2S$) will result in an unstable CO^+ ion, causing its dissociation. The CO^+ ion formed in the single electron capture into the He^+ ($1s\ ^2S$) state will dissociate, leading to the formation of either C^+ or O^+ ion. According to Shah and Gilbody [37], in the collision of He^{2+} ion with CO molecule at 32 keV, the lowest energy they considered in their study, dissociative SEC channels account for a total cross section of 5.05×10^{-16} cm^2 compared with a total of 11.9×10^{-16} cm^2 from the non-dissociative SEC. They also found that the dissociative electron capture leads to the formation of $He^+ + C^+ + O^+ + e^-$, $He^+ + C^{2+} + O + e^-$, $He^+ + C^{2+} + O^+ + 2e^-$ and $He^+ + C^{2+} + O^{2+} + 3e^-$. At 12 keV, Folkerts *et al.* [38] found that fragmentation channels account for about 46 % of total products of the ionization of CO.

IV. Conclusions

The collision dynamics for the $[HeCO]^{2+}$ system has been determined using the impact parameter method [13] in the energy range of 0.6 to 6.0 keV corresponding to a solar-wind ion velocity of about 3 keV at low heliographic latitudes [23]. Partial and total SEC cross sections have been calculated with respect to the statistical weights 1/4 and 3/4 for the singlet and triplet

manifolds, respectively. To understand the effect of molecular orientation on calculated cross sections, the calculation has been performed for He^{2+} ion approaching the carbon and oxygen ends of CO molecule. The dominant contribution of the oxygen end in the electron capture process has been shown. The partial and total SEC cross sections averaged over the two molecular orientations (carbon and oxygen termini) considered in the present calculation have also been given.

The calculated orientation-averaged total single and double electron capture cross sections have been compared with the available experimental results. It has been shown that the impact parameter method provides cross sections which are in good agreement with experimental results [8, 9] in the range of energy considered in the present work. The dominant contribution of the dissociative single electron capture in low-energy collisions has been shown. Single electron capture into He^+ ($1s\ ^2S$) states results in the formation of unstable CO^+ ion and its subsequent fragmentation yielding multiply charged ions has been discussed. The calculated partial and total SEC cross sections illustrate the major role played by radial and rotational couplings compared to spin-orbit couplings. Their influence on processes in the cometary atmosphere leading to X-ray and the EUV photon emission has been demonstrated. The present SEC cross section data should be useful for a variety of applications.

References

[1] S. Lepp, P. C. Stancil, and A. Dalgarno, J. Phys. B: At. Mol. Opt. Phys. **35**, R57 (2002).

[2] T. R. Kallman and P. Palmeri, Rev. Mod. Phys. **79**, 79 (2007).

[3] A. Bhardwaj, R. F. Elsner, G. R. Gladstone, T. E. Cravens, C. M. Lisse, K. Dennerl, G. Branduardi-Raymont, B. J. Wargelin, J. H. Waite Jr., I. Robertson, N. Østgaard, P. Beiersdorfer, S. L. Snowden, and V. Kharchenko, Planet. Space Sci. **55**, 1135 (2007).

[4] I. Yoshikawa, A. Yamazaki, K. Shiomi, M. Nakamura, K. Yamashita, Y. Saito, M. Hirahara, Y. Takizawa, W. Miyake, and S. Matsuura, J. Geophys. Res. **106**, 26057 (2001).

[5] V. A. Krasnoplosky and M. J. Mumma, Astrophys. J. **549**, 629 (2001).

[6] V. A. Krasnopolsky, M. J. Mumma, M. Abbott, B. C. Flynn, K. J. Meech, D. K. Yeomans, P. D. Feldman, and C. B. Cosmovici, Science **277**, 1488 (1997).

[7] D. M. Kearns, D. R. Gillen, D. Voulot, J. B. Greenwood, R. W. McCullough, and H. B. Gilbody, J. Phys. B: At. Mol. Opt. Phys. **34**, 3401 (2001).

[8] T. Kusakabe, Y. Miyamoto, M. Kimura, and H. Tawara, Phys. Rev. A **73**, 022706 (2006).

[9] I. Čadež, J. B. Greenwood, A. Chutjian, R. J. Mawhorter, S. J. Smith, and M. Niimura,

J. Phys. B: At. Mol. Opt. Phys. **35**, 2515 (2002).
[10] K. Ishii, K. Okuno, and N. Kobayashi, Phys. Scr. T **80**, 176 (1999).
[11] M. E. Rudd, T. V. Goffe, and A. Itoh, Phys. Rev. A **32**, 2128 (1985).
[12] M. Albu, L. Mrazek, F. Aumayr, and H. Winter, Int. J. Mol. Sci. **3**, 209 (2002).
[13] R. J. Allan, C. Courbin, P. Salas, and P. Wahnon, J. Phys. B: At. Mol. Opt. Phy. **23**, L461 (1990).
[14] R. J. Buenker, and S. D. Peyerimhoff, Theor. Chim. Acta (Berl.) **35**, 33 (1974).
[15] R. J. Buenker, and S. D. Peyerimhoff, Theor. Chim. Acta (Berl.) **39**, 217 (1975).
[16] R. J. Buenker, Int. J. Quantum Chem. **29**, 435 (1986).
[17] R. J. Buenker, in *Proceedings of the Workshop on Quantum Chemistry and Molecular Physics*, edited by P. G. Burton (University of Wollongong Press, Wollongong, Australia, 1980), p. 1.5.1.
[18] R. J. Buenker, in *Current Aspects of Quantum Chemistry 1981*, edited by R. Carbo, Studies in Physical and Theoretical Chemistry Vol. 21 (Elsevier, Amsterdam, 1982), p.17 and 81.
[19] R. J. Buenker and R. A. Phillips, J. Mol. Struct. (THEOCHEM) **123**, 291 (1985).
[20] S. Krebs and R. J. Buenker, J. Chem. Phys. **103**, 5613 (1995).
[21] R. J. Buenker and S. Krebs, in *Recent Advances in Multireference Methods*, edited by K. Hirao (World Scientific, Singapore, 1999), p. 1.
[22] J. B. Delos, Rev. Mod. Phys. **53**, 287 (1981).
[23] N. A. Schwadron, and T. E. Cravens, Astrophys. J. **544**, 558 (2000).
[24] R. A. Kendall, T. H. Dunning and R. J. Harrison, J. Chem. Phys. **96**, 6796 (1992).
[25] D. E. Woon and T. H. Dunning, J. Chem. Phys. **100**, 2975 (1994).
[26] S. R. Langhoff and E. R. Davidson, Int. J. Quantum Chem. **7**, 759 (1973).
[27] P. J. Bruna, S. D. Peyerimhoff, and R. J. Buenker, Chem. Phys. Lett. **72**, 278 (1980).
[28] K. Kimura, S. Katsumata, Y. Achiba, T. Yamazaki, and S. Iwata, *Handbook of He I Photoelectron Spectra of Fundamental Organic Molecules* (Japan Scientific Society, Tokyo, 1981).
[29] G. Hirsch, P. J. Bruna, R. J. Buenker, and S. D. Peyerimhoff, Chem. Phys. **45**, 335 (1980).
[30] M. Kimura, Y. Li, G. Hirsch, and R. J. Buenker, Phys. Rev. A **52**, 1196 (1995).
[31] B. H. Bransden and M. R. C. McDowell, *Charge Exchange and the Theory of Ion-Atom Collisions* (Clarendon Press, Oxford, 1992), p. 63-64.
[32] P. C. Stancil, B. Zygelman, and K. Kirby, in *Photonic, Electronic, and Atomic Collisions*, edited by F. Aumayr and H. P. Winter (World Scientific, Singapore, 1998), p. 537.
[33] G. D. Billing and M. Baer, Chem. Phys. Lett. **48**, 372 (1977).
[34] H. O. Folkerts, T. Schlathölter, R Hoekstra, and R. Morgenstern, J. Phys. B: At. Mol. Opt. Phys. **30**, 5849 (1997).
[35] L. F. Errea, L. Méndez, and A. Riera, J. Phys. B: At. Mol. Phys. **15**, 101 (1982).
[36] K. P. Huber and G. Herzberg, *Molecular Spectra and MolecularStructure*, Constants of Diatomic Molecules Vol. 4 (Van Nostrand Reinhold, New York, 1979).
[37] M. B. Shah and H. B. Gilbody, J. Phys. B: At. Mol. Opt. Phys. **23**, 1491 (1990).
[38] H. O. Folkerts, F. W. Bliek, M. C. de Jong, R. Hoekstra, and R. Morgenstern, J. Phys. B: At. Mol. Opt. Phys. **30**, 5833 (1997).